Intraoperative detection of micrometastases in whole excised lymph nodes using fluorescent paired agent imaging principles: identification of a suitable staining and rinsing protocol

Chengyue Li<sup>1</sup>, Veronica C. Torres<sup>1</sup>, Yusheng He<sup>1</sup>, Xiaochun Xu<sup>2</sup>, Yusairah Basheer<sup>1</sup>, Georgia Papavasiliou<sup>1</sup>, Kimberley S. Samkoe<sup>2</sup>, Jovan G. Brankov<sup>3</sup>, Kenneth M. Tichauer<sup>1</sup>

- 1. Biomedical Engineering, Illinois Institute of Technology, Chicago, IL, 60616
- 2. Theyer School of Engineering, Dartmouth College, NH, 03755
- 3. Electrical and Computer Engineering, Illinois Institute of Technology, Chicago, IL, 60616 \*Corresponding Author: Kenneth M. Tichauer, Email: ktichaue@iit.edu

#### **ABSTRACT**

**Purpose:** Correctly identifying nodal status is recognized as a critical prognostic factor in many cancer types and is essential to guide adjuvant treatment. Currently, surgical removal of lymph nodes followed by pathological examination is commonly performed as a standard-of-care to detect node metastases. However, conventional pathology protocols are time-consuming, yet less than 1% of lymph node volumes are examined, resulting in a 30-60% rate of missed micrometastases (0.2-2mm in size).

**Procedures:** This study presents a method to fluorescently stain excised lymph nodes using paired-agent molecular imaging principles, which entail co-administration of a molecular targeted imaging agent with a suitable control (untargeted) agent, whereby any nonspecific retention of the targeted agent is accounted for by the signal from the control agent. Specifically, it was demonstrated that by dual-needle continuous infusion of either an antibody-based imaging agent pair (epidermal growth factor receptor (EGFR) targeted agent: IRDye-800CW labeled Cetuximab;

control agent: IRDye-700DX-IgG), or an Affibody-based pair (EGFR targeted Affibody® agent: ABY-029; control agent IRDYe-700DX carboxylate) at 0.3 ml/min.

**Results:** The results demonstrated the possibility to achieve >99% sensitivity and >95% specificity for detection of a single micrometastasis (~0.2 mm diameter) in a whole lymph node within 22 min of tissue processing time.

Conclusion: The detection capabilities offer substantial improvements over existing intraoperative lymph node biopsy methods (e.g., frozen pathology has a micrometastasis sensitivity <20%).

### **Keywords**

Micrometastases, paired-agent, intraoperative imaging, lymph node

#### Introduction

Identification of cancer spread to tumor-draining lymph nodes through lymph node dissection and histology offers critical information for staging and prognosis in many cancer types—including breast, melanoma, head and neck, lung, and gynecologic cancers [1]—as the lymphatic system serves as the primary route for metastasis [2]. Standard clinical practice evaluates lymph node status through surgical removal and histological assessment for cancer cell presence [3]. Exact protocols vary slightly amongst cancer types. In breast cancer, histological evaluation of lymph nodes entails cutting of excised lymph nodes at 2-mm intervals, fixing and embedding all segments, and examining hematoxylin-and eosin (H&E)-stained 5-micron-thick sections from the surface of each segment, which are manually searched by a pathologist for the presence of tumor cell clusters that exceed 0.2 mm in diameter (defined as micrometastases) [3]. This was designed to ensure that

all "macrometastases"—metastases greater than 2 mm in diameter—are detected. However, only the representative sections are evaluated, resulting in an evaluation of the lymph node that includes only about 1% of node's volume. Nearly all nodes with macrometastases are correctly diagnosed; however, it is estimated that 30-60% of patients with micrometastases are misdiagnosed as cancerfree [4, 5]. And while the importance of micrometastases for clinical staging remains controversial, the whole procedure of conventional pathology including gross sectioning, fixing, embedding, fine sectioning, H&E staining, and pathologist reading are considered labor-intensive and require long processing times (> 24 h). This means that if surgeons desire more immediate feedback (for instance if they are evaluating a sentinel node to decide whether to take more nodes in a protocol like targeted axillary dissection in breast cancer [6]), they must currently rely on frozen section pathology and touch prep cytology that offer faster estimates of cancer presence, but with reduced sensitivity to macrometastases of only 60-75% [7-9], and a sensitivity to micrometastases of <20% [10].

As mentioned, the prognostic value of lymph node micrometastases detection remains controversial; however, many reviews suggest that the presence of micrometastases have an adverse effect and their presence is associated with poorer prognoses [11-14]. Micrometastasis detection could identify patients who are at risk of tumor recurrence and might benefit from adjuvant treatment. Many technologies have demonstrated improved detection of micrometastases compared to pathology that could enable early intervention for guiding treatment decisions, such as immunohistochemistry (IHC), serial sectioning, and reverse-transcriptase PCR (RT-PCR) [15-17]. Yet, these methods still rely on either sampling only a small fraction of the lymph node volume

(IHC), are inefficient (e.g., serial sectioning), or involve digestion of the tissue such that subsequent pathology and direct assessment are impossible (e.g., RT-PCR).

The drawbacks of the routine pathologic examination have prompted efforts to seek a more sensitive and "intraoperative" (i.e., can be carried out in a short enough amount of time such that surgical decisions can be made while the patient is still in the operating room) way to identify lymph node status. Our lab developed a paired-agent imaging approach by employing a control imaging agent to allow rapid, quantitative mapping of microscopic cancer cells in lymph nodes to guide pathology. The principles of the approach are based on promising findings in *in vivo* lymph node paired agent imaging using fluorescence, which exhibit detection of micrometastases in rodent models [18, 19]. More recently, we demonstrated the potential to map micrometastases in whole human-sized excised lymph nodes using an enhanced form of fluorescence optical projection tomography for immediate node evaluation or to guide pathologists to suspicious volumes [20, 21]. In this study, the goal was to develop and optimize a staining and rinsing protocol using a paired-agent approach to non-destructively achieve the contrast necessary to detect and localize micrometastases within excised lymph nodes. Antibody conjugate IRDye-800CW-Cetuximab and IRDye-700DX-IgG were used in a paired-agent antibody staining test study and Affibody small molecule ABY-029 [22] and IRDye-700DX carboxylate were used in a pairedagent micro-dose Affibody staining test study, all in excised swine lymph nodes.

#### Materials and methods

# Cell culture

The human breast cancer cell line MDA-MB-231 (ATCC, Mansassas, VA) was used in the experiment. MDA-MB-231 cells were cultured in Dulbecco's modified Eagle medium (DMEM, Corning, NY) with supplements of 10% fetal bovine serum (FBS, HyClone, Logan, Utah) and 1% Penicillin/Streptomycin (Gibco, Grand Island, NY) at 37 °C in a humidified atmosphere of 5% CO<sub>2</sub> in air.

# Green fluorescence protein transfection

The human breast cancer cell line MDA-MB-231 was stably transfected with green fluorescent protein (GFP) plasmid DNA (pAcGFP-N1, Clontech, CA) to allow validation of cancer cells using a previously described method [23]. Briefly, stable transfection was performed using Lipofectamine 3000 (Invitrogen, Grand Island, NY) according to manufacturer instructions. Allowing cells to grow and express GFP, drug selection with G418 (Gibco, Grand Island, NY) was started 72 h after transfection. The survival of cultured mammalian cells expressing GFP was monitored under a fluorescence microscope and the stably expressing cells were confirmed 3 weeks after the selection.

# **Spheroid formation**

Tumor spheroids are now favorable in translational oncology as the 3D architecture can better recapitulate the *in vivo* microenvironment morphologically and physiologically [24-28]. Spheroids were formed *in vitro* by using methylcellulose in medium. Methylcellulose stock solution was prepared prior to generating cell spheroids. 1.2 g of methylcellulose (Sigma, St. Louis, MO) were autoclaved in a 250-mL glass bottle with a magnetic stirrer inside. A volume of 50 mL preheated basal medium (60 °C) was added to the autoclaved methylcellulose and the mixture was placed in

a water bath on a hot plate at  $60^{\circ}\text{C}$  for 20 min (magnetic stirrer was used to facilitate the dissolution process). Subsequently, another 50 mL of basal medium was added and the combined solution was mixed overnight at  $4^{\circ}\text{C}$ . The solution was aliquoted and centrifuged for 2 h at  $4^{\circ}\text{C}$  and 4000 RPM. The final stock solution was collected by taking the supernatant of about 90% of the centrifuged product. When the cells reached between 80-90% confluence, Trypsin/EDTA 1X (Corning) was used to detach adherent cells from their monolayer. Cells were then suspended in culture medium containing 0.24% (w/v) methylcellulose (mixture of 80% culture medium and 20% methylcellulose stock solution);  $150~\mu\text{L}$  of cell suspension medium containing  $\sim 1\times 10^4$  cells were seeded in each well of round-bottom, non-tissue treated 96 well-plates (Falcon, NY) and incubated for 3 days. Spheroid formation was confirmed under bright field microscopy, while GFP expression was verified under a fluorescence microscope (Axiovert 200, Zeiss, Thornwood, NY).

# Sample preparation

Swine neck tissues were freshly dissected and obtained from a local butcher shop in Chicago, IL on the day of experiments. Swine cervical lymph nodes were excised, and any excess fat was trimmed immediately prior to experimental protocols. A total of 24 lymph nodes were resected.

#### Experimental micrometastatic lymph node model

To mimic the clinical condition of micrometastases in a tumor draining lymph node, an experimental micrometastatic lymph node model was developed by implanting ~0.2 mm diameter tumor spheroids (smallest cell cluster that would be characterized as a micrometastasis) in swine lymph nodes. Tumor spheroids were transferred from medium to a 1.5-mL microcentrifuge tube (Thermo Fisher Scientific) via micropipette and collected by gravitation. Culture medium was

removed, and spheroids were washed twice with PBS, then resuspended in fresh PBS solution. A 23-gauge syringe-needle (BD PrecisionGlide Needle) was used for implantation considering the size in diameter of culture cancer spheroids ranged from 200 to 300 µm. Spheroids were collected one at a time using the micropipette and carefully aspirated into the syringe, aiming to restrain the spheroid within the needle tip. The needle tip was then inserted into the lymph node with bevel facing up, and 5 µL PBS containing a spheroid was slowly injected. After injection, the syringe was held in place for 1 min and the tip was rotated 180 degree (i.e. the bevel facing downward) before retracting the needle. Trial and error revealed that a careful and slow withdrawal of the needle was critical to avoid reflux of the injected fluid and spheroid. One to two spheroids were implanted in each 8 of the resected lymph nodes.

# **Imaging agents**

#### Antibody

Cetuximab (provided by Davis Lab at Dartmouth College), an EGFR-specific antibody, was selected to act as a targeted imaging agent, labeled with a near-infrared fluorophore IRDye-800CW (LI-COR Biosciences, Inc., Lincoln, NE). A non-targeted negative control antibody, Rat immunoglobin G (IgG, MP Biomedicals, Santa Ana, CA), was labeled with IRDye-700DX (LI-COR Biosciences, Inc., Lincoln, NE) as a control agent. Both antibodies were labeled with the NHS ester form of the fluorophore using manufacturer-supported protocols as previously described [19]. In brief, the fluorophore was added to the antibody solution in a 5:1 dye-to-antibody ratio at pH 8.5 for optimal binding. The solution was then covered with aluminum foil to protect it from light and was maintained under gentle stirring for 2 h at room temperature. The dye-protein conjugate was then isolated using a 40K Pierce Zeba desalting spin column (Thermo

Fisher Scientific). Once the free dye was sufficiently removed, the dye-to-protein ratio of the final conjugate was determined with a NanoDrop 2000 spetrophotometer (Thermo Fisher Scientific).

#### *Affibody*

The Good Laboratory Practices (GLP) synthesized ABY-029 stock solutions were provided by the Samkoe lab at Dartmouth College [22] and were further diluted in sterile PBS for experimental administration. ABY-029, an anti-EGFR Affibody molecule labeled with IRDye-800CW, was paired with IRDye-700DX carboxylate, a non-targeted small molecule imaging agent. The IRDye-700DX carboxylate was converted from IRDye-700DX NHS ester as per instructions from the manufacturer, by dissolving IRDye-700DX NHS in PBS at a pH of 8.5. The solution was protected from light and gently stirred at room temperature for 5 h.

# Intranodal infusion staining/rinsing

Two 23-gauge butterfly needles (BD Vacutainer blood collection set) were pierced into opposite sides of the lymph node on its longest axis and lymph nodes were immersed in PBS solution to retain moisture levels. The needles were taped to avoid movement during the staining and rinsing process. Infusion solution was delivered via a 12-inch tube that connected the needle to syringe at an infusion rate of 0.3 ml/min controlled by a dual-syringe infusion pump (KD Scientific, Holliston, MA). Lymph nodes were pre-washed with 300 μL of 2% (w/v) BSA (bovine serum albumin, Sigma-Aldrich) in PBS prior to measurement in order to remove excess blood that enhanced autofluorescence. A pre-staining image was then acquired by a Pearl Imaging System (LICOR Bioscience, Lincoln, NE) to evaluate the background levels caused by autofluorescence. A 300-μL volume of 1:1 imaging agent mixture of 200-nM IRDye-800CW-Cetuximab and IRDye-

700DX-IgG for antibody staining test and 2-nM ABY-029 and IRDye-700DX carboxylate for affibody micro-dose staining test, was mixed with 2% (w/v) BSA in PBS and infused into the lymph nodes at 0.3 mL/min at both sites for 1 min. Immediately after staining, white-light and fluorescence at 700-740 nm and 800-840 nm (from 685 and 785 nm excitation, respectively) were acquired on the Pearl Imaging System. At 15 min after administrating the imaging agents, lymph nodes were then infused with PBS at the same infusion rate for 5 min. During the rinsing process, all lymph nodes were imaged at 1-min intervals to monitor the fluorescence of targeted and control imaging agents.

#### **Serial section examinations**

The post-staining/rinsing lymph nodes were flash frozen and serial sectioning was performed on a cryostat microtome (Shandon Cryotome E, Thermo Electron Corp., Marietta, OH) at 200-µm intervals. The sectioned tissues were mounted onto slides and immediately imaged under an 85-µm resolution fluorescence imaging system (Pearl Impulse, LICOR Biosciences). The fluorescence of targeted and control imaging agents in the cross-sectional lymph nodes were collected and the spatial distribution of both imaging agents were compared. The tissue slides were then fixed with 10% neutral buffered formalin (Sigma-Aldrich) at 4°C. All slides of spheroid-implanted lymph nodes were imaged on a confocal microscopy at 488 nm excitation and 525 nm emission wavelengths (PASCAL LM5, Zeiss, Thornwood, NY) to identify the location of cancer spheroids by green fluorescence protein (GFP) expression.

### Paired-agent imaging

The paired-agent imaging estimates the targeted biomolecule concentration by employing a control imaging agent to account for non-specific uptake and retention of targeted imaging agent concentration [29-31]. By making the assumption that the control imaging agent signal approximates the free concentration of the targeted imaging agent, the binding potential can be calculated using:

$$BP = \frac{I_T}{I_C \times NF} - 1 \tag{1}$$

where  $I_T$  and  $I_C$  are the pixel intensity of the targeted and control imaging agents, respectively, and NF is the normalization factor determined by

$$NF = \frac{\bar{I}_T}{\bar{I}_C} \tag{2}$$

where  $\bar{I}_T$  and  $\bar{I}_C$  are the average pixel intensities of the selected targeted and control imaging agents, respectively, in a diluted stock staining solution imaged on the same device used for the experiments. The dilution factor matched the expected dilution of stock solution into the lymph nodes: specifically 0.3 ml (volume of staining solution) divided by 3 ml (estimated volume of an average, ~8-mm-diameter spherical lymph node).

### **Image analysis**

Images were analyzed using in-house code written in MATLAB (R2018b, MathWorks, Natick, MA). For whole-node data analyses, pre-injection images were subtracted from all post-injection images (following motion correction) to remove the effects of background autofluorescence. The fluorescence signals of the targeted and NF-scaled control imaging agents were compared to evaluate their concentration and the BP (from Eq. (1)) in intact lymph nodes as a function of time. Circular region-of-interest (ROIs) of 0.2-mm-diameter were placed on GFP identified tumor spheroids, a GFP-negative area of the lymph node, and normal lymph nodes to evaluate the

detection ability using BP maps. The images of targeted agent, control agent, and BP maps collected with the Pearl System at 85-µm resolution were co-registered to the GFP images collected on confocal microscopy at 3.5-µm resolution by first resizing the GFP images to 85-µm resolution. The images of the binding potential map were then co-registered with the GFP images by manually aligning lymph node edges perceivable in both BP and GFP images in MATLAB. Receiver operating characteristic (ROC) curves were then calculated in MATLAB for further comparison.

#### Statistical analysis

To evaluate the strength of correlation of targeted agent and control agent over time in normal (cancer free) lymph nodes, a linear regression was performed node-by-node, the strength of which was quantified by the average Pearson's correlation coefficient, and statistical significance of the correlation was determined by comparing the individual correlation slopes from each node (independent subjects) against a slope of 0 [32]. A repeated-measured ANOVA, with time as a within-subjects variable and binding potential value as a between-subjects variable, was used to identify the presence of statistically significant differences between temporal binding kinetics of micrometastatic lymph node and normal lymph nodes. Paired *t*-tests were performed to determine statistical significance of the differences in BP between micrometastatic regions, normal regions of micrometastatic lymph nodes and normal lymph nodes. As for diagnostic parameter, area under the curve (AUC) of the receiver operating characteristic (ROC) curve, sensitivity, and specificity for pixel-based analyses were determined based on their mathematic formula using a 10% intensity threshold in GFP images as a gold standard for presence or absence of cancer in any given pixel (note: while not an exact gold standard measure, this arbitrary thresholding allows comparison of

diagnostic accuracy between targeted fluorescence alone and paired-agent binding potential methods) [33]. All data are presented as mean  $\pm$  standard deviation, and statistical significance was set at p < 0.05.

#### **Results**

### Intranodal infusion staining/rinsing

Control lymph nodes

To test the feasibility of using the paired-agent intranodal infusion staining and rinsing protocol with intact lymph nodes, the equivalence of the targeted and control imaging agents of normal lymph nodes were assessed over time throughout the staining and rinsing process (1 min rinse, 1 min stain infusion, 15 min wait time, 5 min rinse—which was identified as promising through trial and error experiments). Normal lymph nodes (n = 8) with no spheroids implanted were evaluated with antibody and Affibody staining test (n = 4 with antibody staining test: using 200 nM IRDye-800CW labeled Cetuximab as targeted agent and IRDye-700DX labeled IgG as control agent; n = 4 with Affibody staining test: using 2 nM ABY-029 as targeted agent and IRDye-700DX carboxylate as control agent).

Figure 2(a) and (b) present the measured time courses of the pair of IRDye-800CW-Cetuximab and IRDye-700DX-IgG, and ABY-029 and IRDye-700DX carboxylate, respectively, during the infusion rinsing process. On average, the stained solution reached 70% washout in 5 min rinsing by infusion. The results of the washout kinetics of the targeted agent and control agent demonstrated a statistically significant correlation with each other for both antibody and Affibody

(r = 0.99, p < 0.001). The temporal retention of the targeted and control agents were not statistically different by repeated-measured ANOVA test.

### Micrometastatic lymph node model

To evaluate the feasibility of using this paired-agent staining approach to detect micrometastases in excised lymph nodes, a total of 8 nodes were implanted with 200-300- $\mu$ m-diameter human cancer cells spheroids. Four "micrometastatic" lymph nodes were infused with equivalent molar mixed solutions of IRDye-800CW-Cetuximab and IRDye-700DX-IgG at a concentration of 200 nM, while 4 nodes were infused with a 1:1 mixture of ABY-029 and IRDye-700DX carboxylate at micro-dose concentration of 2 nM. Figure 2(c) and (d) display the measured time-courses of fluorescence from both targeted and control imaging agent in micrometastatic lymph node models of antibody study (n = 4) and Affibody study (n = 4), respectively. The kinetic curves exhibited slightly higher fluorescence retention of the targeted agent signal compared to the control agent in the presence of cancer. However, the fluorescence of targeted and control agent did not change significantly over time by repeated-measured ANOVA test.

Figure 3(e) and (f) summarizes the average binding potential of IRDye-800CW-Cetuximab and ABY-029, respectively with comparison between micrometastatic and control lymph node models over time. Binding potential of micrometastatic lymph node models in the two studies increased over time and repeated-measured ANOVA analysis demonstrated that the binding potential of both IRDye-800CW-Cetuximab and ABY-029 in micrometastatic lymph node models had statistically significant differences from normal lymph nodes after 5-min infusion rinsing (p < 0.05). It should be noted that this data was obtained under premixing 2% albumin in the imaging cocktail solution;

otherwise, the signal of both imaging agents failed to correlate consistently with each other in both tests with antibody and Affibody by only mixing imaging agents alone in PBS as shown in Figure 2 (g) and (h) (n = 4 for each paired-agent testing).

#### Cross-sectional lymph node analyses

To further analyze the spatial distribution of the paired imaging agents within the lymph nodes after the infusion staining/rinsing protocol, post-procedure lymph nodes were rapidly frozen and underwent serial cryosections of 200-um thickness. Figure 3 presents representative images of paired-agent fluorescence and BP maps from one normal lymph node and one micrometastatic lymph node from the antibody staining test. Fluorescence images of control agent (IRDye-700DX-IgG, shown in red) and targeted agent (IRDye-800CW-Cetuximab, shown in green) of a normal lymph node are presented in Fig 3(a) and (b), respectively. These images display the distribution of the control and targeted agents were nearly identical in the control lymph node, and the fluorescence of both targeted and control agent exhibited a higher retention in certain regions. However, after binding potentials were calculated on a pixel-by-pixel basis shown in Fig 3(c), the binding potential map demonstrated no significant higher value within the lymph node. In the case of micrometastatic lymph node, higher uptake of imaging agent was observed in both control targeted agent (shown in Fig 3(e) and (f), respectively). The binding potential map shown in Fig 3(g) illustrates that the binding potential of IRDye-800-Cetuximab in the presence of binding was significantly higher, coinciding with measurable GFP-expressing cancer cells as identified by the fluorescence microscope image. To evaluate the ability of binding potential maps to be used to detect cancer, 0.2-mm-diameter circular ROIs were placed on GFP identified tumor spheroids, a GFP-negative area of the lymph node, and normal lymph nodes. Mean BP values from these

regions were  $1.8 \pm 0.8$ ,  $0.0 \pm 0.4$  and  $-0.1 \pm 0.3$ , respectively. One-way ANOVA was performed and the binding potential of micrometastatic regions were found to have a statistically significant difference from both normal regions in tumor-bearing lymph nodes, and normal lymph node regions (p < 0.05), while no significant difference between the group of normal regions and normal lymph nodes was observed.

As Affibody molecules are much smaller in size than antibodies, and have favorable properties for diagnostic application, a 1:1 mixed solution of 2 nM IRDye-800CW labeled affibody, ABY-029 and IRDye-700DX carboxylate was used to test the feasibility of a microdosing Affibody staining approach. Figure 4 shows the representative images of paired-agent fluorescence and BP maps from one normal lymph node (top row) and one micrometastatic lymph node (bottom row) in the Affibody-microdose staining test group. Fig 4(a) and (e) shown in red display the fluorescence of control imaging agent (IRDye-700DX carboxylate) and Fig 4(b) and (f) shown in green display the fluorescence of targeted imaging agent (ABY-029). The corresponding binding potentials were calculated, and the results demonstrated that the binding potential of normal lymph nodes remained low and relatively homogeneous within the entire lymph node sections evaluated, as presented in Fig(c), while the micrometastatic lymph nodes exhibited significantly higher signal at locations with GFP-verified cancer present (Fig. 4(g)). As with the antibody groups, ROIs were placed on tumor regions and tumor-free background regions in cancer-bearing and cancer-free nodes. The results showed that the mean micrometastatic region BPs  $(1.8 \pm 0.8)$  were significantly greater than mean BPs measured from different normal region ( $-0.05 \pm 0.08$ ) and normal lymph nodes (- $0.01 \pm 0.09$ ) (p < 0.05).

# Micrometastases detection performance

The serial sections of BP images were stacked for visualization to provide quasi-3D viewing of binding potential maps of entire sectioned lymph nodes. Fig 5(a) presents a 3D representation of binding potential of a representative micrometastatic lymph node from the antibody infusion group. Two spheroids were implanted in the lymph node and one of the sections with spheroid deposition was selected for demonstration purposes. The fluorescence of control agent (IRDye-700DX-IgG, shown in red), fluorescence of targeted agent (IRDye-800CW-Cetuximab, shown in green), calculated BP map and green fluorescence protein expression image are shown in Fig 5(a). Fig 5(b) demonstrates an overlay image of co-registered BP map and GFP image, which were used to identify a cancerous region to plot a receiver-operating characteristic (ROC) curve. The diagnostic ability of the control agent fluorescence, targeted agent fluorescence and BP maps are illustrated in the ROC curve presented in Fig 5(c). The results demonstrated both BP and IRDye-800CW-Cetuximab showed better evaluation ability than IRDye-700DX-IgG, and BP exhibited a slightly higher area-under-the ROC curve (AUC) value than IRDye-800CW-Cetxuximab alone (quantified for the whole groups in the next section).

Fig 5(d) presents a 3D lymph node BP map, control agent fluorescence (IRDye-700DX carboxylate, shown in red), targeted agent fluorescence (ABY-029, shown in green), binding potential map and corresponding GFP fluorescence image of a representative section of a micrometastatic lymph node in Affibody microdose-infusion study. The BP map with overlays of green fluorescence protein fluorescence for cancer cell identification is presented in Fig 5(e). The plotted ROC curve shown in Fig 5(f) demonstrates BP has a higher AUC value of the ROC curve

than either ABY-029 and IRDye-700 carboxylate alone (quantified for the whole groups in the next section).

### Diagnostic ability of paired-agent infusion staining protocol

To further evaluate the diagnostic ability of paired-agent staining versus using a single targeted imaging agent with the infusion staining protocol, Table 1 presents quantitative metrics of diagnostic accuracy amongst groups. Note: the optimal threshold for each spheroid deposited section was chosen by maximizing the sum of sensitivity and specificity using ROC curves [34]. BP in both antibody and Affibody studies exhibited higher AUC, sensitivity and specificity than targeted agent alone.

Table 1. Diagnostic parameters of lymph node sections

	Antibody		Affibody	
_	ВР	IRDye-800CW- Cetxuimab	BP	ABY-029
AUC	0.97 ± 0.04	0.94 ± 0.09	0.989 ± 0.006	0.96 ± 0.03
Optimal Threshold	1.5 ± 0.9	$0.002 \pm 0.002$	$0.9 \pm 0.5$	0.0006 ± 0.0005
Sensitivity	$0.99 \pm 0.03$	$0.9 \pm 0.1$	1.0 ± 0.0	$0.98 \pm 0.03$
Specificity	$0.90 \pm 0.09$	0.9 ± 0.1	$0.94 \pm 0.03$	$0.89 \pm 0.05$

All lymph nodes were grouped into cohorts with different imaging type (antibody and Affibody) shown in Fig 6. In the antibody staining test with IRDye-800CW-Cetuximab and IRdye-700DX-IgG at concentration of 200 nM, Fig 6(a) demonstrates that higher AUC of the ROC curves of BP (shown in blue) than IRDye-800CW-Cetximab (shown in green) was observed. Sensitivity and specificity are presented along with the differences of threshold presented in Fig. 6(b) for BP and

6(c) for IRDye-800CW-Cetuximab. The summation of sensitivity and specificity were also plotted for optimizing the threshold such that the maximum percentage of true presence and absence were correctly identified. Fig 6(d) displays the measured performance of microdose Affibody infusion staining test group with 2 nM mixture of ABY-029 and IRDye-700DX carboxylate by plotting the ROC curves. The higher AUC of ROC curves of BP indicated that the paired-agent infusion staining approach using microdose Affibody had higher performance in prediction than ABY-029 alone. Fig 6(e) and (f) plot the performance of BP and ABY-029 along with the threshold selection.

In the cohort statistic shown in Table 2, the BP in both antibody and Affibody studies exhibited overall higher performance in AUC of the ROC curves, sensitivity and specificity. Specifically, AUC of the ROC curve of BP in both studies demonstrated statistically significant higher values than targeted agent alone (AUC of ROC curves were 0.966 for the BP of antibody and 0.787 for IRdye-800CW-Cetuximab, p < 0.0001; AUC of ROC curves were 0.985 for the BP of Affibody and 0.740 for ABY-029, p < 0.0001). While Affibody staining test was performed at a much lower dose than antibody, the AUC of the ROC curves of BP using 2 nM ABY-029 was statistically significantly higher than BP using 200 nM IRDye-800CW-Cetuximab.

Table 2. Diagnostic parameters of cohort statistics

	Antibody		Affibody	
-	ВР	IRDye-800CW- Cetxuimab	ВР	ABY-029
AUC	0.97	0.79	0.99	0.74
Optimal Threshold	1.06	0.002	0.93	0.0007
Sensitivity	0.91	0.58	0.99	0.61
Specificity	0.89	0.86	0.92	0.78

#### **Discussion**

The status of cancer-draining lymph nodes is recognized as one of the most significant prognostic factors to stage many cancer types. The presence of cancer cells and the number of positive lymph nodes can indicate the extent of disease, and are essential to guide the optimal treatment for patients. However, conventional histopathological examination practice examines only 1% of a whole lymph node, such that many micrometastases can be overlooked leading to false-negative diagnoses [4, 5]. Moreover, standard pathology can require days to process, and faster methods suffer from greater false-positive rates. In response to the limitations in standard lymph node pathology, our group is aiming to develop a method to nondestructively detect and map micrometastases in whole excised lymph nodes to provide intraoperative feedback to surgeons with lower false-negative rates than observed with frozen-section pathology. In addition to the development of a lymph node fluorescence optical tomography system [20], an important step in this objective is the development of a methodology to fluorescently "stain" whole lymph nodes, which is the focus of the current work. The feasibility of using this paired-agent methodology to stain lymph nodes by submerging the tissue in staining solution has been evaluated with healthy rat and human lymph nodes[35]. The results demonstrated the spatial distribution of two imaging agents show strong correlation with each other in the cancer-free lymph nodes. However, this traditional staining strategy required long staining time to reach full permeation of intact lymph nodes. Numerous whole mount staining methods have been developed to accelerate the staining process of intact tissue specimen by utilizing pressure, temperature, electric fields, and probe chemistry [36-38]. For instance, active clarity technique—pressure related efficient and stable transfer macromolecules into organs (ACT-PRESTO)—can facilitate active penetration of macromolecules, such as antibodies, deep into dense organs by applying centrifugal pressure or

convection flow to organs [36], resulting in expediated staining time of 3 hours for 120 µm thick tissue specimens. However, these approaches still require staining duration ranging from a few hours to days, which are not suitable for intraoperative cancer diagnostics. After much trial-and-error (testing whole-lymph node submersion, split lymph node submersion, and various whole-lymph node intranodal infusion staining and rinsing strategies), this study presents a staining and rinsing methodology allowing >4 times reduction in staining/rinsing time compared to submersion approaches, capable of evenly staining and rinsing intact lymph nodes at <25 min of total process time while providing sufficient detection accuracy.

Several factors were considered to design the intranodal infusion staining strategy. Owing to the heterogeneous internal structure of lymph nodes—which contain various compartments including cortex and follicles—the nonspecific uptake of the targeted agent was expected to spatially vary substantially within the lymph node. Moreover, owing to the nature of injection involving needle insertion and the dynamic variation at different locations in the infusion system, non-homogeneous distribution of the imaging agent caused by injection was also expected. The paired-agent methodology was selected to account for these effects by, in effect, normalizing the targeted imaging agent retention in any region to the level of nonspecific retention represented by the level of control agent present (targeted and control agents being simultaneously infused). Note that paired agent imaging requires some measurable delivery of agents to all areas of interest, and an incomplete washing of the tissue (i.e., some control agent must be left behind). In this study, the lowest measured control agent fluorescence after rinsing in all nodes was >4 times the maximum autofluorescence signal measured (results not shown). This suggests (1) both antibody-based and Affibody-based agents exhibited sufficient delivery to all areas of the whole lymph nodes, and (2)

while the rinsing strategy employed was sufficient to produce measurable proportional differences in targeted and control agent concentrations at locations of cancer, it was not strong enough to yield sufficient signals of control agent that would have made the paired-agent ratiometric strategy (Eq. 1) stable.

Fig 5(d) provides a stark example of the importance of paired agent imaging for such an application. In the targeted fluorescence image, two regions of substantial florescence uptake were observed, presumably implying the presence of cancer at both locations. However, only one of the high-signal areas actually corresponded to cancer cells present (as determined by GFP images corregistered by lymph node surface landmarks perceivable on both the Pearl and Microscopy systems). This region exhibited proportionately higher targeted fluorescence than control agent fluorescence. On the other hand, the cancer free "hot spot" exhibited both high targeted fluorescence and control agent fluorescence, indicating that this "hot spot" was only from nonspecific accumulation. The binding potential map—from Eq. (1) and which is equivalent to an estimate of the targeted receptor concentration multiplied by the imaging agent affinity [30, 39]—offers a visual representation of this correction method, correctly identifying only the fluorescence hot spots correlating to the cancer presence.

The overall improvements in tumor discrimination possible with paired-agent imaging compared to single agent imaging in this application are further verified by the significant improvements in AUC of the ROC, maximum sensitivity + specificity, achievable for paired-agent binding potential maps compared to single agent fluorescence alone (Fig 5, 6, and Table 1 and 2). With predicted single micrometastasis detection sensitivities of greater than 95% and specificities of greater than

90% for both antibody and Affibody based approaches, such methods have the potential to far outperform standard breast cancer node pathology (>40% micrometastasis false-negative rates [4, 5]) and frozen section pathology (>80% micrometastasis false-negative rates [10]), in less time required than either of these established methods. Since early studies suggest that the staining/rinsing procedure does not interfere with the quality of subsequent pathology (to be presented in future work), it can be directly compared with pathology in future clinical studies (as opposed to destructive protocols such as RT-PCR) [42]. In order to aid in the potential for wide clinical adoption, further evaluation of larger lymph nodes (diameters greater than 15 mm) will be performed to investigate the protocol effectiveness with the lymph node size variation. Moreover, the feasibility of minimal manipulation such as gently compressing the tissue will be evaluated as a means to enhance the detection performance using our fluorescence optical projection tomography. Moreover, while these initial results demonstrate an ability to use <25 min tissue processing to reach sensitivity and specificity matching 24 h+ conventional pathology, future optimization in the protocol can be explored through accurate simulations of imaging agent diffusion and binding in lymph nodes. Such efforts may require modeling of heterogeneous internal structures of lymph nodes, imaging agent properties, and pressure gradients during infusion governing the fluid convection. Such a model would have similarity to infusion treatments that have been modeled in glioma [40, 41].

It should be noted that considering the smaller molecule size of Affibody that possess favorable properties in diffusion and diagnostics, a microdose of ABY-029 at the concentration of 2 nM was tested while the antibody staining group utilized a 100-times higher concentration at 200 nM IRDye-800CW-Cetuximab. Despite the much lower dose of the Affibody, the AUC of BP of

Affibody solution at 2 nM demonstrated a statistically significant higher performance than antibody at 200 nM in cohort analysis (p<0.001). The superior performance of the microdose Affibody might be the result of their faster rates of binding and smaller size compared to the antibody [22], which would allow for fast diffusion and washout in this intranodal infusion staining protocol within the short staining/rinsing time. Further investigation of comparing different Affibody concentration using the intranodal infusion staining protocol could be performed to evaluate the optimal Affibody concentration in order to achieve the highest contrast-to-noise ratio (CNR) in tumor discrimination; however, this study at least demonstrates the feasibility of using either antibody-based imaging agents or much smaller, Affibody-based agents to achieve detection metrics with paired-agent imaging far exceeding that estimated with competing and existing intraoperative lymph node assays.

# Conclusion

This study demonstrated the potential of a paired-agent intranodal infusion staining protocol to provide true molecular contrast in distinguishing tumor and healthy tissue in lymph nodes to improve the sensitivity of micrometastasis detection compared to conventional pathology. This time-effective approach will allow pathological evaluation to be performed under intraoperative settings.

#### **Funding**

This work has been funded from National Science Foundation (1653627), Nayar Prize at Illinois Tech and National Cancer Institute NCI R01 CA167413 for the synthesis of ABY-029.

# **Conflict of interest**

Dr. Samkoe reports grants from National Cancer Institute, during the conduct of the study; and ABY-029 was manufactured under National Cancer Institute NCI R01 CA167413 grant as an academic-industrial partnership between Dartmouth College, Affibody AB, and LI-COR Biosciences, Inc.

#### References

- 1. Chen SL, Iddings DM, Scheri RP, Bilchik AJ: Lymphatic mapping and sentinel node analysis: current concepts and applications. *CA Cancer J Clin* 2006, 56:292-309; quiz 316-297.
- 2. Swartz MA, Skobe M: Lymphatic function, lymphangiogenesis, and cancer metastasis. *Microsc Res Tech* 2001, 55:92-99.
- 3. Lyman GH, Giuliano AE, Somerfield MR, Benson AB, 3rd, Bodurka DC, Burstein HJ, Cochran AJ, Cody HS, 3rd, Edge SB, Galper S, et al: American Society of Clinical Oncology guideline recommendations for sentinel lymph node biopsy in early-stage breast cancer. *J Clin Oncol* 2005, 23:7703-7720.
- 4. Weaver DL: Pathology evaluation of sentinel lymph nodes in breast cancer: protocol recommendations and rationale. *Mod Pathol* 2010, 23 Suppl 2:S26-32.
- 5. Tew K, Irwig L, Matthews A, Crowe P, Macaskill P: Meta-analysis of sentinel node imprint cytology in breast cancer. *Br J Surg* 2005, 92:1068-1080.
- 6. Caudle AS, Yang WT, Krishnamurthy S, Mittendorf EA, Black DM, Gilcrease MZ, Bedrosian I, Hobbs BP, DeSnyder SM, Hwang RF, et al: Improved Axillary Evaluation Following Neoadjuvant Therapy for Patients With Node-Positive Breast Cancer Using Selective Evaluation of Clipped Nodes: Implementation of Targeted Axillary Dissection. *J Clin Oncol* 2016, 34:1072-1078.
- 7. Chao C, Wong SL, Ackermann D, Simpson D, Carter MB, Brown CM, Edwards MJ, McMasters KM: Utility of intraoperative frozen section analysis of sentinel lymph nodes in breast cancer. *Am J Surg* 2001, 182:609-615.
- 8. Dixon JM, Mamman U, Thomas J: Accuracy of intraoperative frozen-section analysis of axillary nodes. Edinburgh Breast Unit team. *Br J Surg* 1999, 86:392-395.
- 9. Mitchell ML: Frozen section diagnosis for axillary sentinel lymph nodes: the first six years. *Mod Pathol* 2005, 18:58-61.
- 10. Weiser MR, Montgomery LL, Susnik B, Tan LK, Borgen PI, Cody HS: Is routine intraoperative frozen-section examination of sentinel lymph nodes in breast cancer worthwhile? *Ann Surg Oncol* 2000, 7:651-655.
- 11. Deng XF, Jiang L, Liu QX, Zhou D, Hou B, Cui K, Min JX, Dai JG: Lymph node micrometastases are associated with disease recurrence and poor survival for early-stage non-small cell lung cancer patients: a meta-analysis. *J Cardiothorac Surg* 2016, 11:28.
- 12. Choi SB, Han HJ, Park P, Kim WB, Song TJ, Choi SY: Systematic review of the clinical significance of lymph node micrometastases of pancreatic adenocarcinoma following surgical resection. *Pancreatology* 2017, 17:342-349.
- 13. Zhou Y, Zhang GJ, Wang J, Zheng KY, Fu W: Current status of lymph node micrometastasis in gastric cancer. *Oncotarget* 2017, 8:51963-51969.
- 14. Ferlito A, Partridge M, Brennan J, Hamakawa H: Lymph node micrometastases in head and neck cancer: a review. *Acta Otolaryngol* 2001, 121:660-665.
- 15. Hata M, Machi J, Mamou J, Yanagihara ET, Saegusa-Beecroft E, Kobayashi GK, Wong CC, Fung C, Feleppa EJ, Sakamoto K: Entire-volume serial histological examination for

- detection of micrometastases in lymph nodes of colorectal cancers. *Pathol Oncol Res* 2011, 17:835-841.
- 16. Dhawan I, Sandhu SV, Bhandari R, Sood N, Bhullar RK, Sethi N: Detection of cervical lymph node micrometastasis and isolated tumor cells in oral squamous cell carcinoma using immunohistochemistry and serial sectioning. *J Oral Maxillofac Pathol* 2016, 20:436-444.
- 17. Martin LW, D'Cunha J, Wang X, Herzan D, Gu L, Abraham N, Demmy TL, Detterbeck FC, Groth SS, Harpole DH, et al: Detection of Occult Micrometastases in Patients With Clinical Stage I Non-Small-Cell Lung Cancer: A Prospective Analysis of Mature Results of CALGB 9761 (Alliance). *J Clin Oncol* 2016, 34:1484-1491.
- 18. Tichauer KM, Samkoe KS, Gunn JR, Kanick SC, Hoopes PJ, Barth RJ, Kaufman PA, Hasan T, Pogue BW: Microscopic lymph node tumor burden quantified by macroscopic dual-tracer molecular imaging. *Nat Med* 2014, 20:1348-1353.
- 19. Li C, Xu X, McMahon N, Alhaj Ibrahim O, Sattar HA, Tichauer KM: Paired-Agent Fluorescence Molecular Imaging of Sentinel Lymph Nodes Using Indocyanine Green as a Control Agent for Antibody-Based Targeted Agents. *Contrast Media Mol Imaging* 2019, 2019:7561862.
- 20. Torres VC, Li C, He Y, Sinha L, Papavasiliou G, Sattar HA, Brankov JG, Tichauer KM: Angular restriction fluorescence optical projection tomography to localize micrometastases in lymph nodes. *J Biomed Opt* 2019, 24:1-4.
- 21. Torres VC, Li C, Zhou W, Brankov JG, Tichauer KM: Characterization of an angular domain fluorescence optical projection tomography system for mesoscopic lymph node imaging. *Applied Optics* 2020, 60:135-146.
- 22. Samkoe KS, Gunn JR, Marra K, Hull SM, Moodie KL, Feldwisch J, Strong TV, Draney DR, Hoopes PJ, Roberts DW, et al: Toxicity and Pharmacokinetic Profile for Single-Dose Injection of ABY-029: a Fluorescent Anti-EGFR Synthetic Affibody Molecule for Human Use. *Mol Imaging Biol* 2017, 19:512-521.
- 23. Li C, Xu X, Basheer Y, He Y, Sattar HA, Brankov JG, Tichauer KM: Paired-agent fluorescent imaging to detect micrometastases in breast sentinel lymph node biopsy: experiment design and protocol development. In *Advanced Biomedical and Clinical Diagnostic and Surgical Guidance Systems XVI*. International Society for Optics and Photonics; 2018: 1048402.
- 24. Fennema E, Rivron N, Rouwkema J, van Blitterswijk C, de Boer J: Spheroid culture as a tool for creating 3D complex tissues. *Trends Biotechnol* 2013, 31:108-115.
- 25. Zanoni M, Piccinini F, Arienti C, Zamagni A, Santi S, Polico R, Bevilacqua A, Tesei A: 3D tumor spheroid models for in vitro therapeutic screening: a systematic approach to enhance the biological relevance of data obtained. *Sci Rep* 2016, 6:19103.
- 26. Sant S, Johnston PA: The production of 3D tumor spheroids for cancer drug discovery. *Drug Discov Today Technol* 2017, 23:27-36.
- 27. He YJ, Young DA, Mededovic M, Li K, Li C, Tichauer K, Venerus D, Papavasiliou G: Protease-Sensitive Hydrogel Biomaterials with Tunable Modulus and Adhesion Ligand Gradients for 3D Vascular Sprouting. *Biomacromolecules* 2018, 19:4168-4181.
- 28. He YJ, Santana MF, Moucka M, Quirk J, Shuaibi A, Pimentel MB, Grossman S, Rashid MM, Cinar A, Georgiadis JG, et al: Immobilized RGD concentration and proteolytic degradation

- synergistically enhance vascular sprouting within hydrogel scaffolds of varying modulus. *J Biomater Sci Polym Ed* 2020, 31:324-349.
- 29. Tichauer KM, Wang Y, Pogue BW, Liu JT: Quantitative in vivo cell-surface receptor imaging in oncology: kinetic modeling and paired-agent principles from nuclear medicine and optical imaging. *Phys Med Biol* 2015, 60:R239-269.
- 30. Tichauer KM, Samkoe KS, Sexton KJ, Gunn JR, Hasan T, Pogue BW: Improved tumor contrast achieved by single time point dual-reporter fluorescence imaging. *J Biomed Opt* 2012, 17:066001.
- 31. Li C, Torres VC, Tichauer KM: Noninvasive detection of cancer spread to lymph nodes: A review of molecular imaging principles and protocols. *J Surg Oncol* 2018, 118:301-314.
- 32. Tichauer KM, Hadway JA, Lee TY, St Lawrence K, Lawrence KS: Measurement of cerebral oxidative metabolism with near-infrared spectroscopy: a validation study. *J Cereb Blood Flow Metab* 2006, 26:722-730.
- 33. Swets JA: Measuring the accuracy of diagnostic systems. *Science* 1988, 240:1285-1293.
- 34. Manel S, Williams HC, Ormerod SJ: Evaluating presence—absence models in ecology: the need to account for prevalence. *Journal of Applied Ecology* 2001, 38:921-931.
- 35. Li C, Torres V, Xu X, Basheer Y, Sattar H, Brankov J, Tichauer K: *Protocol development of paired-agent fluorescent imaging to detect micrometastases in resected breast lymph nodes*. SPIE; 2019.
- 36. Lee E, Choi J, Jo Y, Kim JY, Jang YJ, Lee HM, Kim SY, Lee H-J, Cho K, Jung N: ACT-PRESTO: Rapid and consistent tissue clearing and labeling method for 3-dimensional (3D) imaging. *Scientific reports* 2016, 6:18631.
- 37. Yang B, Treweek JB, Kulkarni RP, Deverman BE, Chen C-K, Lubeck E, Shah S, Cai L, Gradinaru V: Single-cell phenotyping within transparent intact tissue through whole-body clearing. *Cell* 2014, 158:945-958.
- 38. Susaki EA, Tainaka K, Perrin D, Yukinaga H, Kuno A, Ueda HR: Advanced CUBIC protocols for whole-brain and whole-body clearing and imaging. *Nature protocols* 2015, 10:1709.
- 39. Innis RB, Cunningham VJ, Delforge J, Fujita M, Gjedde A, Gunn RN, Holden J, Houle S, Huang SC, Ichise M, et al: Consensus nomenclature for in vivo imaging of reversibly binding radioligands. *J Cereb Blood Flow Metab* 2007, 27:1533-1539.
- 40. Bobo RH, Laske DW, Akbasak A, Morrison PF, Dedrick RL, Oldfield EH: Convection-enhanced delivery of macromolecules in the brain. *Proceedings of the National Academy of Sciences* 1994, 91:2076-2080.
- 41. Allard E, Passirani C, Benoit J-P: Convection-enhanced delivery of nanocarriers for the treatment of brain tumors. *Biomaterials* 2009, 30:2302-2318.
- 42. Nolan T, Hands RE, Bustin SA: Quantification of mRNA using real-time RT-PCR. *Nature protocols* 2006, 1:1559-1582.

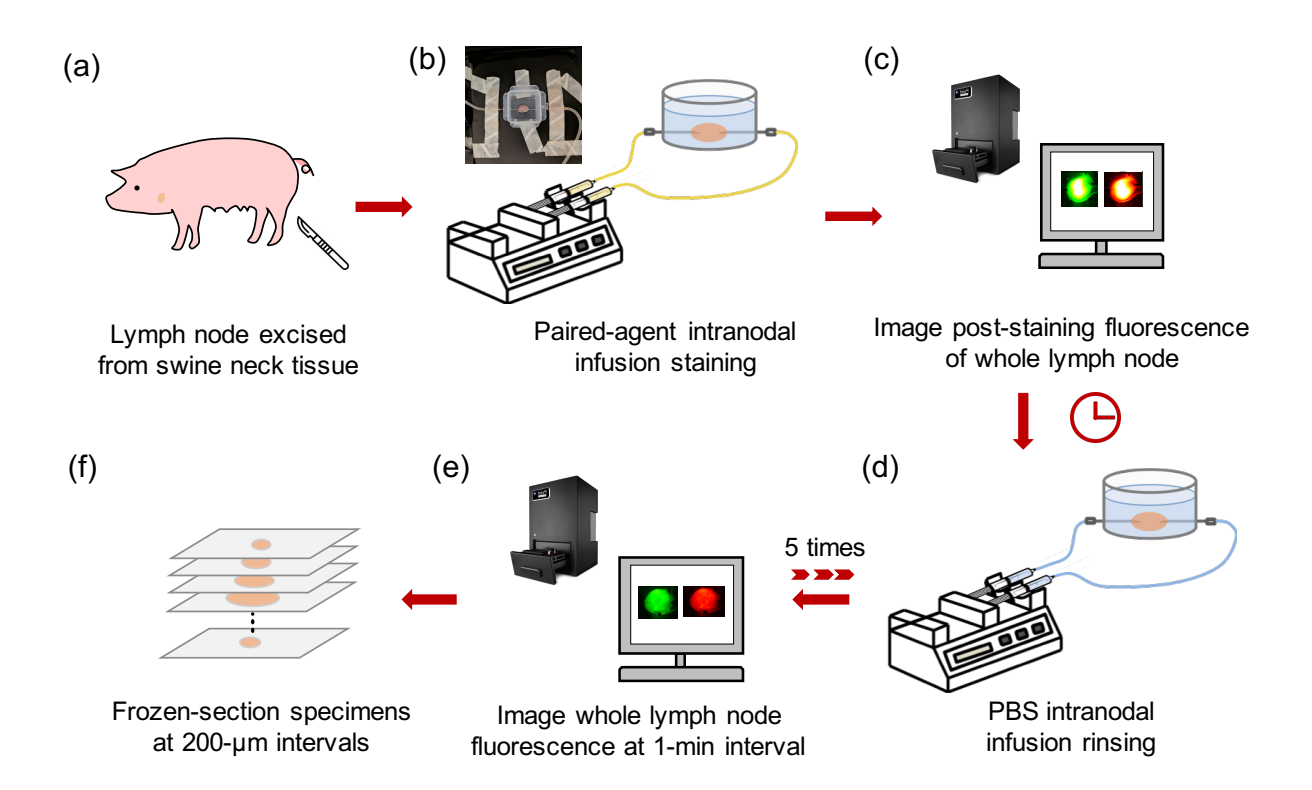


Figure 1. Stepwise illustration of lymph node paired-agent intranodal infusion staining and rinsing protocol. (a) Swine lymph nodes were excised and (b) infused with paired-agent imaging agents via intranodal infusion controlled by syringe pump; lymph nodes were submerged in PBS to retain moisture levels. (c) Post-staining fluorescence of lymph nodes were recorded immediately after the 1-min staining process. (d) After 15 min, lymph nodes were rinsed with PBS and (e) the whole lymph node fluorescence signals were monitored at 1-min intervals. (f) Lymph nodes were then frozen-sectioned at 200-μm intervals to evaluate the spatial distribution of both imaging agents in the lymph nodes.

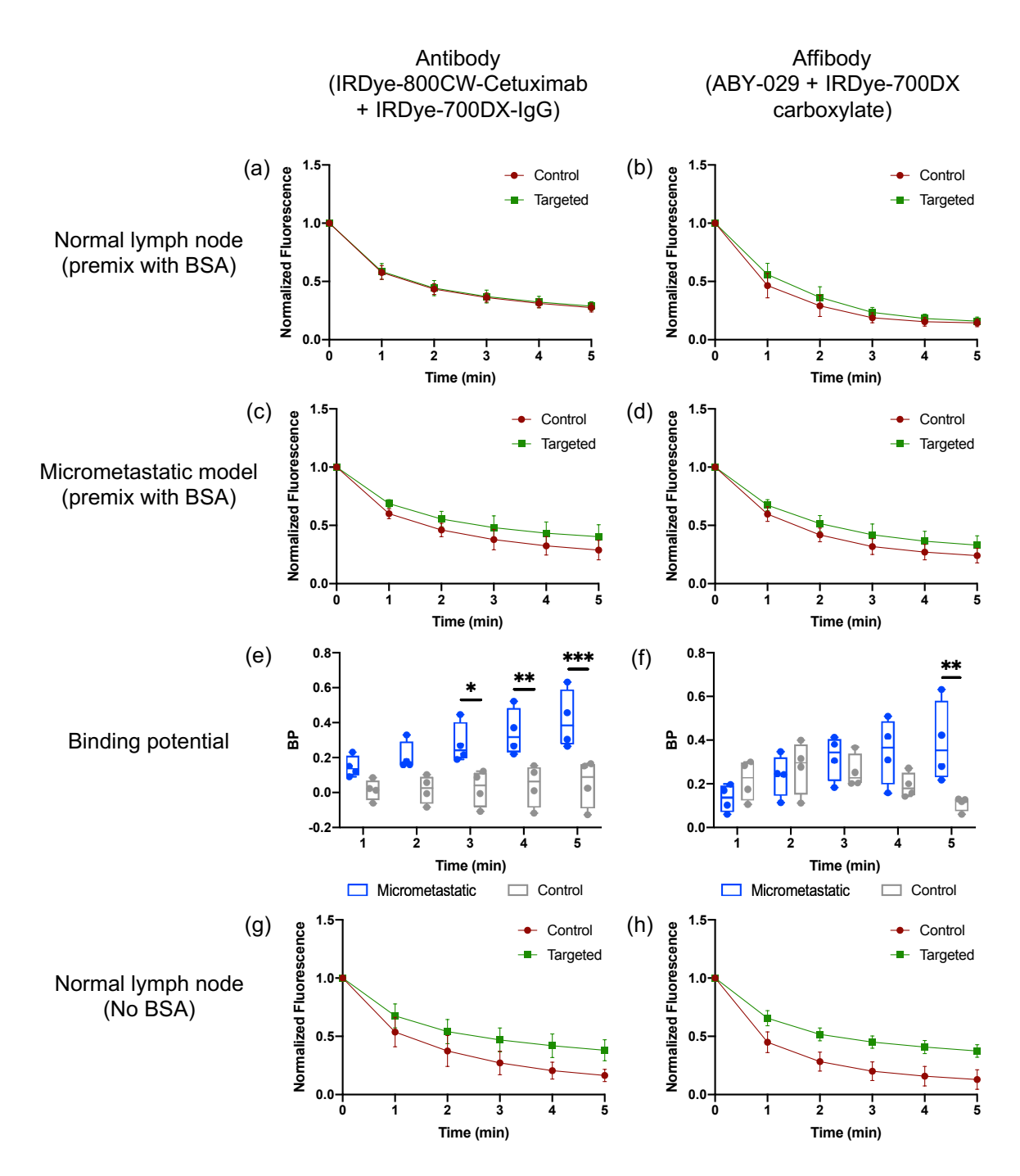


Figure 2. Overview of kinetics of antibody and Affibody paired-agents imaging in control and micrometastatic lymph node models using intranodal infusion staining/rinsing protocol. The potential ability of paired-agent imaging agents to be stained and washed to produce similar kinetics via intranodal infusion are presented in (a) and (b). (c) and (d) exhibited the potential of this protocol to detect micrometastases in tumor-draining lymph nodes. The average binding potential as a function of time for various micrometastatic lymph nodes and control lymph nodes are presented in (e) and (f). The time course of fluorescence from targeted and control imaging agents failed to correlate with each other in the absence of albumin in the imaging agent solution as shown in (g) and (h).

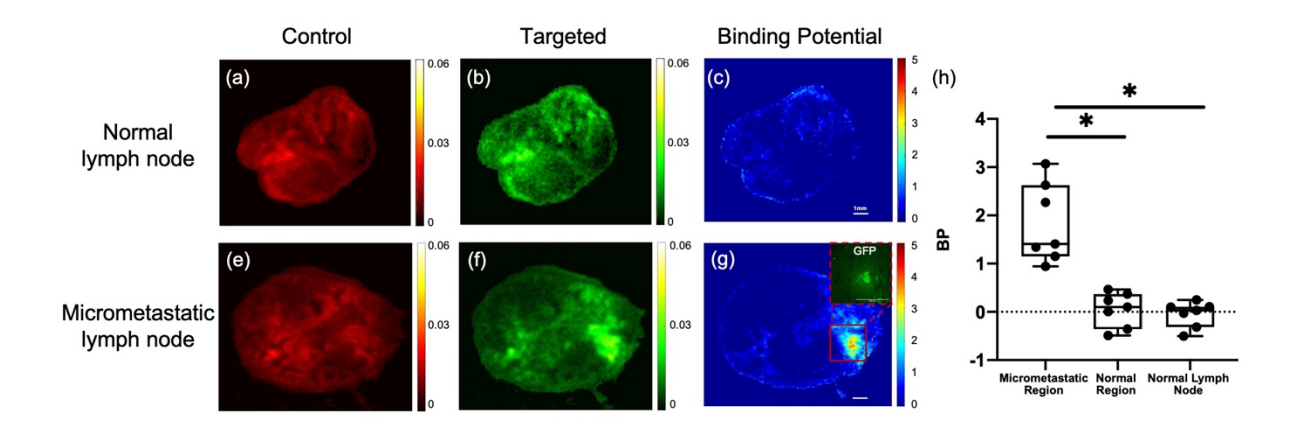


Figure 3. An overview of cross-sectional lymph node images of antibody infusion staining test. (ac) present fluorescence images of control agent (red), targeted agent (green) and binding potential map of a normal lymph node. (e) shows the control agent distribution and (f) shows the antibody-targeted agent distribution in a tumor-bearing lymph node, and the binding potential map presented in (g) shows higher signal in a region indicating the presence of cancer cells (GFP-expression verified). (h) demonstrates the differences of average binding potential of IRDye-800CW-Cetuximab with group of ROIs placed on tumor-bearing nodes with cancer presence ("metastatic regions"), with no cancer ("normal region"), and in non-tumor-bearing nodes. (\* p < 0.05)

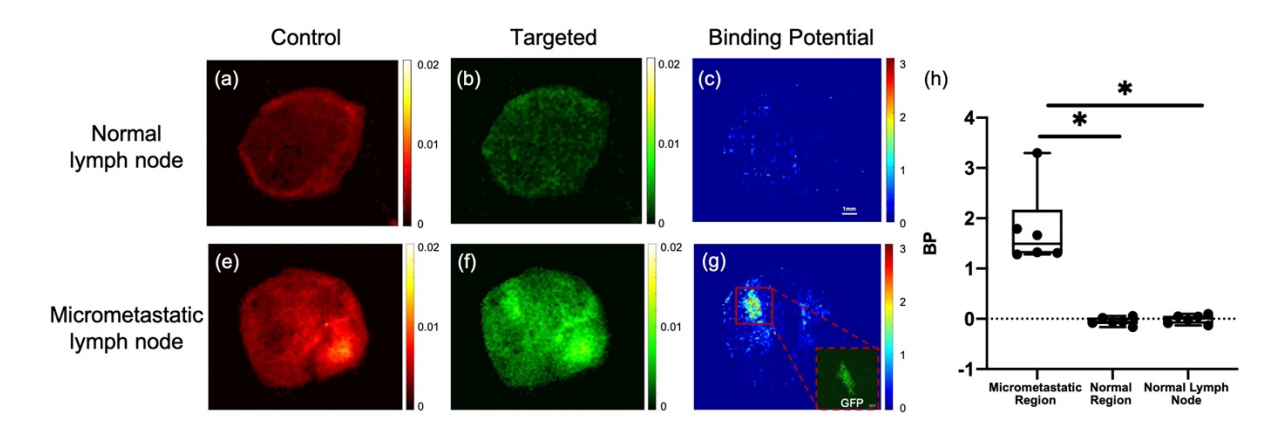


Figure 4. An overview of cross-sectional lymph node images of Affibody-microdose infusion staining test. The uptake of both imaging agents in the entire lymph node are shown in (a) and (b) of a normal lymph node, and (e) and (f) of a cancer spheroid implanted lymph node. The binding potential map of the normal lymph node is presented in (c) in the absence of binding, while confirmed presence of cancer spheroid match the location that higher binding potential was observed in the cancer bearing node binding potential map, shown in (g). (h) demonstrated the differences of average binding potential of ABY-029 amongst a group of ROIs placed on tumor-bearing nodes with cancer presence ("metastatic regions"), with no cancer ("normal region"), and in non-tumor-bearing nodes.

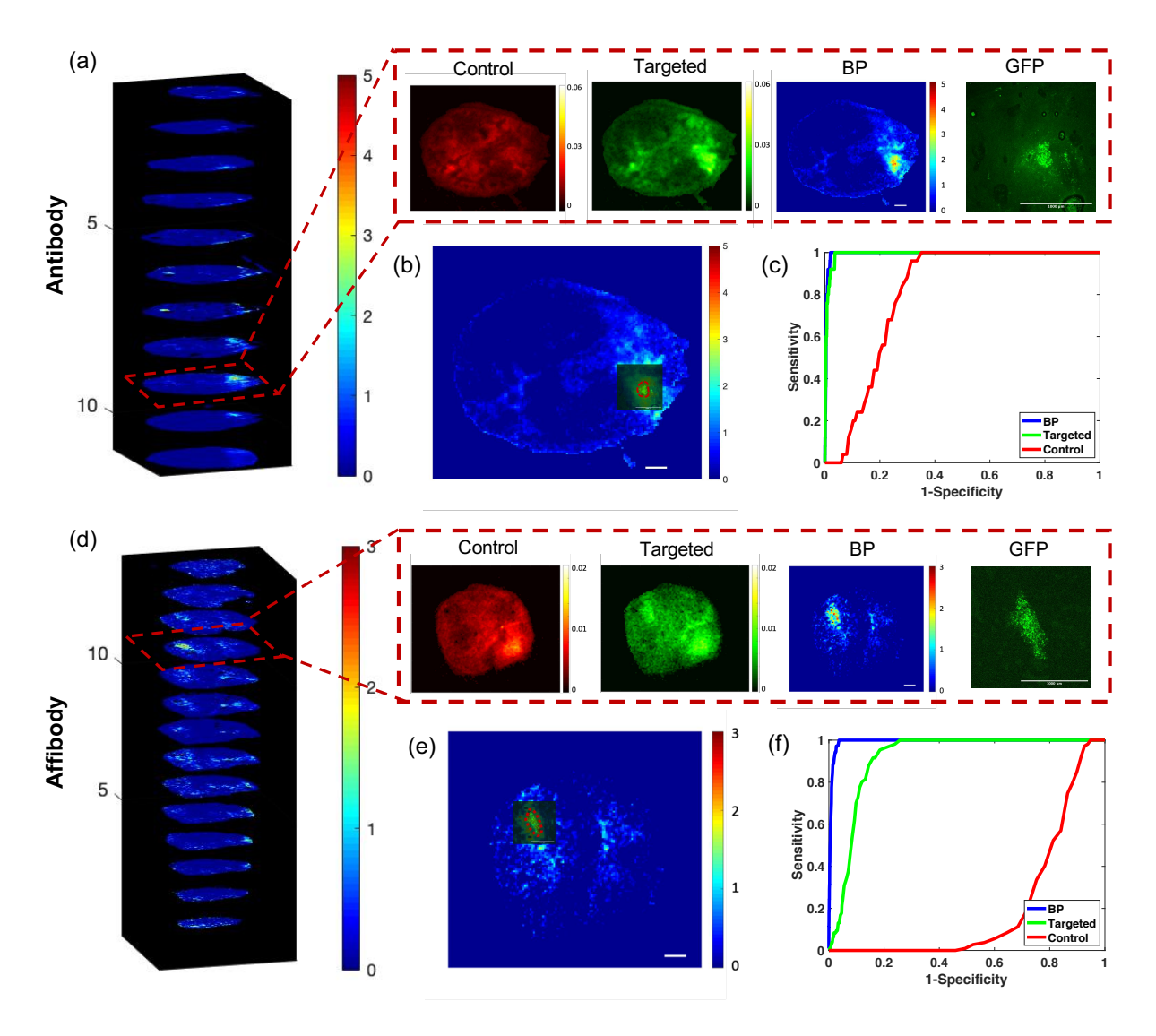


Figure 5. The micrometastases detection evaluation of representative sections in both antibody and Affibody staining test groups. (a) and (d) present the images of 3D mapping of lymph nodes, control agent fluorescence (red), targeted agent fluorescence (green), BP map and GFP fluorescence image of antibody staining and Affibody staining test, respectively. (b) and (e) present the overlay images of co-registered BP map and GFP expression used to calculate the ROC curves shown in (c) and (f) to evaluate micrometastases detection performance of intranodal infusion staining protocol.

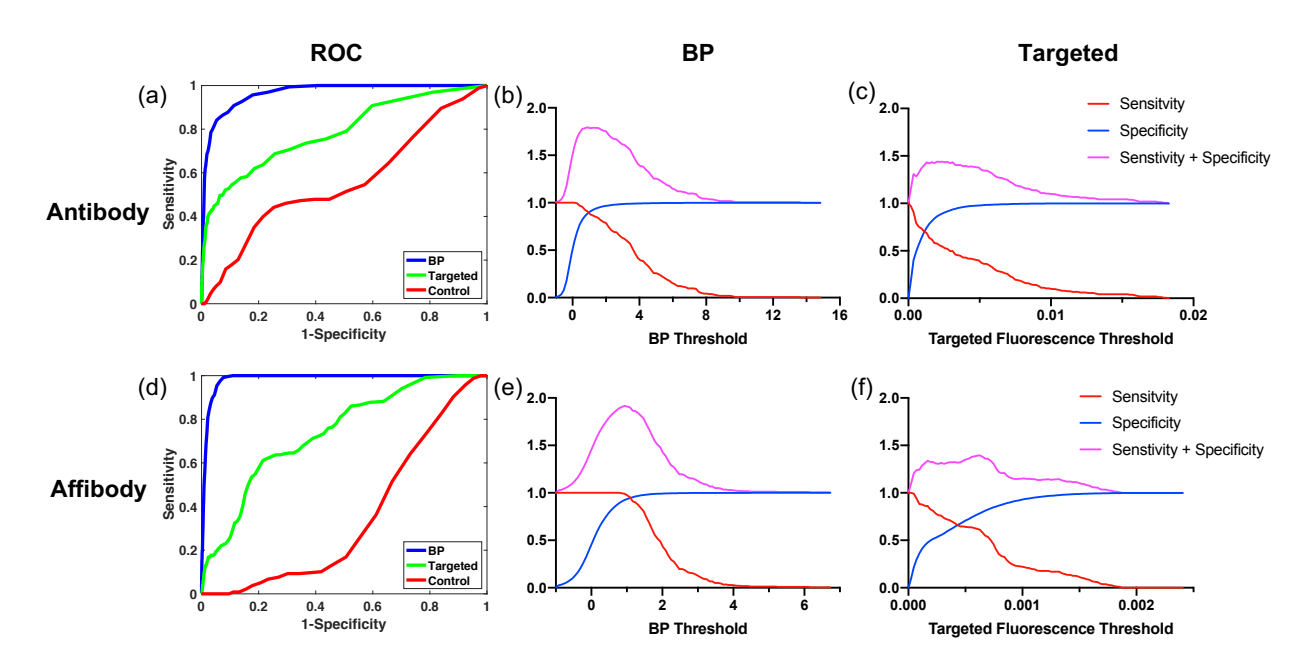


Fig 6. Overall performance of BP and targeted agent alone with intranodal infusion staining protocol in antibody (presented in top row) and micro-dose Affibody (presented in bottom row) tests. Fig (a) and (d) demonstrate the receiver operating characteristic (ROC) curves of BP (shown in blue), targeted agent (shown in green), and control agent (shown in red). Figure (b-c) and (e-f) show sensitivity and specificity plotted along with parameter threshold of BP of antibody, IRDye-800CW-Cetuximab, BP of Affibody and ABY-029, respectively.